AIP | Applied Physics Letters

Enhanced thermoelectric performance in the very low thermal conductivity Ag2Se0.5Te0.5

Fivos Drymiotis, Tristan W. Day, David R. Brown, Nicholas A. Heinz, and G. Jeffrey Snyder

Citation: Applied Physics Letters **103**, 143906 (2013); doi: 10.1063/1.4824353
View online: http://dx.doi.org/10.1063/1.4824353
View Table of Contents: http://scitation.aip.org/content/aip/journal/apl/103/14?ver=pdfcov
Published by the AIP Publishing

Enhanced thermoelectric performance in the very low thermal conductivity $Ag_2Se_{0.5}Te_{0.5}$

Fivos Drymiotis,[a] Tristan W. Day, David R. Brown, Nicholas A. Heinz, and G. Jeffrey Snyder
Department of Materials Science, California Institute of Technology, Pasadena, California 91125, USA

(Received 24 July 2013; accepted 22 September 2013; published online 3 October 2013)

In this letter, we report the high-temperature thermoelectric properties of $Ag_2Se_{0.5}Te_{0.5}$. We find that this particular composition displays very low thermal conductivity and competitive thermoelectric performance. Specifically, in the temperature region $520\,K \leq T \leq 620\,K$, we observe non-hysteretic behavior between the heating and cooling curves and zT values ranging from 1.2 to 0.8. Higher zT values are observed at lower temperatures on cooling. Our results suggest that this alloy is conducive to high thermoelectric performance in the intermediate temperature range, and thus deserves further investigation. © *2013 AIP Publishing LLC*. [http://dx.doi.org/10.1063/1.4824353]

Devices based on thermoelectric (TE) materials convert heat into electricity in a compact and robust package with no moving parts. Development of higher efficiency thermoelectric materials, as determined by the dimensionless figure-of-merit zT is crucial to grid-scale implementation of thermoelectrics for waste heat conversion (e.g., from industrial exhaust) and grid scale electrical generation (e.g., solar thermal). The figure-of-merit is determined by the relative values of heat and electrical transport properties: $zT = \alpha^2 T/\rho\kappa$ (figure-of-merit), where α is the Seebeck coefficient or thermopower, ρ is the electrical resistivity, κ is the thermal conductivity, and T is the temperature.[1] Maximum thermoelectric conversion efficiency can be achieved by maximizing α, while minimizing ρ and κ. However, as these properties are interrelated through the physics and chemistry of the materials, it is not possible to engineer these properties separately. Certain classes of materials tend to display good thermoelectric performance; for example, the binary and ternary chalcogenides provide a low thermal conductivity platform combined with low electrical resistivity leading to a high zT. An examination of the current state-of-the-art thermoelectric materials reveals that the chalcogenides have many representatives (PbTe,[2] Bi_2Te_3,[3] TAGS,[4,5] Sb_2Te_3,[6] and $AgSbTe_2$.[7,8]) The binary silver chalcogenides (Ag_2Se and Ag_2Te) have not gained as much attention even though previous reports[9–13] indicate that they are very promising materials. For example, the thermoelectric performance of Ag_2Se is rather high; $zT = 0.96$ at $T = 300\,K$,[9] and recent work showed that proper synthesis procedure leads to a substantial improvement of the thermoelectric performance of Ag_2Te.[14] Since, at room temperature, Ag_2Te stabilizes in a monoclinic structure, while Ag_2Se stabilizes in an orthorhombic structure,[15] it is worth exploring the stoichiometry $Ag_2Se_{0.5}Te_{0.5}$ in order to assess whether phase competition and subsequent complexity can improve thermoelectric performance.[16] Because of the competing structures, we expect that for specific x, phase separation will occur on solidification, leading to the formation of a complex composite with very low thermal conductivity possibly like those found in Refs. 17 and 18. Indeed, this is what can be inferred from the Ag_2Se-Ag_2Te phase diagram (Figure 1).[19]

Ag, Te, and Se, all of purity 99.9999% were placed in quartz tubes in the molar ratio 2:0.5:0.5. The quartz tubes were then evacuated, sealed, and placed inside a box furnace. The samples were subsequently heated to 1000 °C, where they were allowed to remain for 5 h, before finally being allowed to cool down to 300 °C at a rate of 10 °C/h, at which point the power to the furnace was turned off. The formed ingots were removed from the quartz tubes and processed for measurement. Disks of 8-mm diameter and approximately 2-mm thickness were cut from the ingots. The measured density of the disks was $d = 8.2\,g/cm^3 \pm 5\%$. The structures were confirmed using X-ray diffraction data obtained using a commercial Rigaku MiniFlex® diffractometer. The thermal diffusivity was obtained using the Netzsch LFA 457® laser flash apparatus. The thermal conductivity values were calculated for each sample using the relation $\kappa = DdC_p$, with D being the measured diffusivity value, d the density, and C_p the heat capacity at constant pressure. The value of d used in the calculations was the measured density at room temperature for the various samples. The value of C_p was taken to be the value of the Dulong-Petit limit. The Seebeck coefficient[20] and the electrical resistivity and Hall effect[21] were measured on equipment designed for this purpose at the California Institute of Technology.

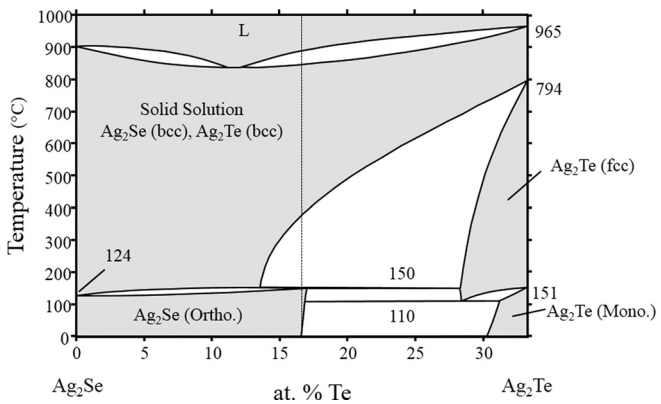

FIG. 1. The Ag_2Se-Ag_2Te phase diagram. The dark gray vertical line corresponds to the 0.5/0.5 composition.

[a]Email: fivos@caltech.edu

According to the X-ray diffraction data (Figure 2(a), black line), the dominant structure is the orthorhombic Ag_2Se. The Rietveld refinement (Figure 2(a), red line) was performed using the program Rietica and the structural model $P2_12_12_1$ (space group 19). The lattice parameters obtained from the fit are $a = 4.4330$ Å, $b = 7.2345$ Å, and $c = 7.9676$ Å. The corresponding lattice parameters for the stoichiometric Ag_2Se (Ref. 22) are $a = 4.330$ Å, $b = 7.062$ Å, and $c = 7.764$ Å. The 2.5% increase in the lattice parameters is expected since Te is larger than Se. Traces of a secondary phase might still be present but not in a sufficient amount to be detected by X-ray diffraction. The corresponding reduction in the thermal conductivity between the stoichiometric and heavily doped phase is also shown (Figure 2(b)). The thermal conductivity of Ag_2Te is also shown for comparison. The X-ray data are consistent with the Ag_2Se-Ag_2Te phase diagram (Figure 1), which shows that for this particular composition and temperature (16.67 at. % Te and room temperature), the alloy consists of substituted orthorhombic Ag_2Se and traces of doped monoclinic Ag_2Te.

Both Ag_2Se and Ag_2Te undergo a structural phase transition in the intermediate temperature region;[15,19] the former from orthorhombic to bcc at 124 °C and the latter from monoclinic to fcc at 151 °C), and both compounds display ionic conductivity above the transition[23] (Ag_2Te undergoes an additional transition from fcc to bcc at 794 °C). According to the phase diagram,[19] for the 0.5/0.5 composition (16.67 at. %, dark gray vertical line in Figure 1) and cooling from 1000 °C, the sample enters a solid-solution region at approximately 860 °C; (the liquid-solid region above 860 °C is neglected since slowly cooling to 300 °C will allow the mixture to settle to a solid-solution). However, at approximately 380 °C, the sample reaches the solid-solution solvus line at which point the Ag_2Te (Se doped) fcc phase begins to precipitate. With further cooling the mixture finally enters a single-phase orthorhombic Te-doped Ag_2Se region (~150 °C).

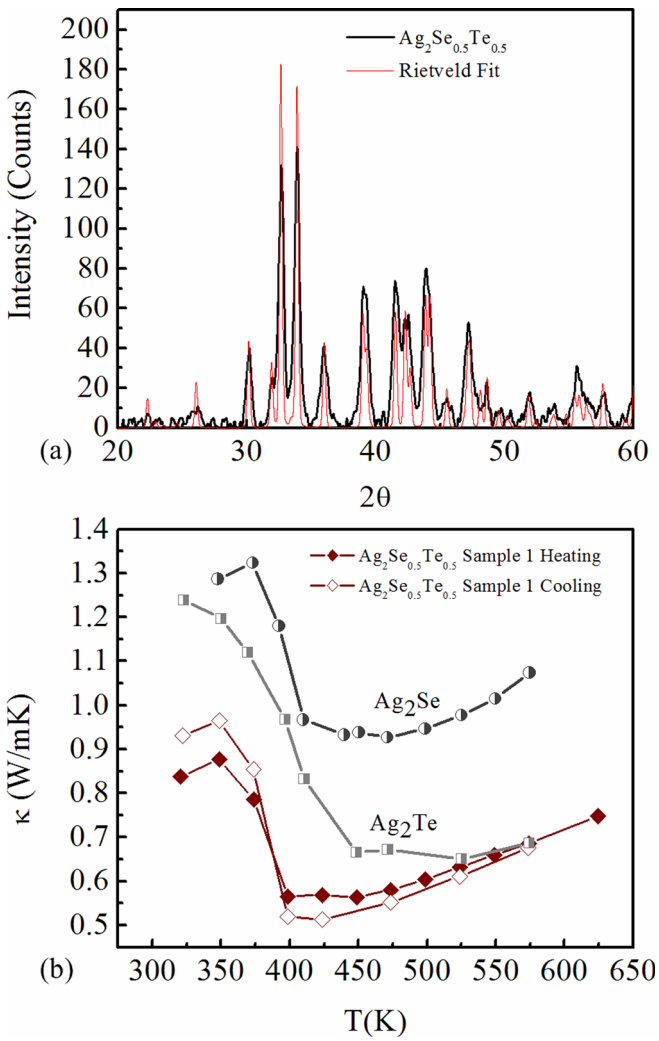

FIG. 2. (a) X-ray diffraction data of an ingot sample of $Ag_2Se_{0.5}Te_{0.5}$ (black spectrum). The Rietveld refinement is also displayed for comparison (red spectrum). (b) Thermal conductivity of orthorhombic Ag_2Se, monoclinic Ag_2Te and of $Ag_2Se_{0.5}Te_{0.5}$ (sample 1).

Because of the super-ionic transition and the complex structure, the electrical transport properties must be measured carefully and consistently. A large hysteresis is observed in both the electrical resistivity and Seebeck data during the first heating and cooling cycle through the transition. This large hysteresis may lead to high zT values that may not be reproducible. However, cycling the sample through the transition causes the hysteresis to be eliminated between 520 K and 620 K and to become consistent between 440 K and 520 K. The hysteresis is presumably due to the multiple phases that are represented in the Ag_2Se-Ag_2Te phase diagram.[19] Thus, in order to assess the thermoelectric potential of this composition, we performed measurements on multiple samples, while following a consistent protocol. The procedure was as follows: (1) we performed the Seebeck measurements first and cycled the samples 2 to 3 times through the transition and up to a maximum temperature of 350 °C, (2) we performed the thermal diffusivity measurements and cycled the samples only once through the transition and up to a maximum temperature of 350 °C, and (3) we performed the resistivity and Hall measurements, cycling the samples 2 to 3 times through the transition and up to a maximum temperature of 350 °C. The samples were measured up to a maximum temperature of 350 °C in order to avoid entering the solid solution region; entering the solid-solution region results in a permanent change in the transport properties. The dimensionless figure-of-merit was calculated using the thermal diffusivity data and the resistivity and Seebeck data obtained during the last measurement cycle for each sample. All samples showed similar behavior and comparable zT values. Presented is the dimensionless figure-of-merit for all 3 samples measured. For brevity, the electrical and thermal transport data are presented from only sample 1.

The general features of the thermal and electrical transport behavior of these samples are such that the thermal conductivity decreases as the samples go through the structural phase transition, while the magnitude of the thermopower and the electrical resistivity (Figures 3(a) and 3(c)) increase. Above the transition, the electrical resistivity values remain rather low (<3 mΩ-cm), the magnitude of the thermopower increases and the thermal conductivity assumes values that are much less than 1 W/mK. Hence, this particular composition is conducive to high thermoelectric performance.

The thermal conductivity of this alloy is extremely low (Figure 2(b)). The reduction in total thermal conductivity in the case of $Ag_2Se_{0.5}Te_{0.5}$, when compared to both Ag_2Se and

Ag_2Te is rather dramatic. Since both Ag_2Se and $Ag_2Se_{0.5}Te_{0.5}$ share the same structure and undergo a similar structure transformation, it implies that the reduction in thermal conductivity in the case of $Ag_2Se_{0.5}Te_{0.5}$ is due to point defect scattering.[24] The total thermal conductivity at room temperature remains <1 W/mK and it decreases as the sample goes through the structural phase transition. It reaches a minimum value of <0.6 W/mK at $\sim$420 K before it starts increasing monotonically at high temperatures due to the presence of minority carriers. At approximately 575 K, the thermal conductivity value of $Ag_2Se_{0.5}Te_{0.5}$ equals that of Ag_2Te.

In the case of the thermopower (Figure 3(a)), the absolute value of the Seebeck coefficient decreases considerably after the first temperature cycle. However, it assumes a relatively constant value ($\alpha \sim -160\,\mu$V/K) for a wide temperature range. During all cycles, the magnitude of the Seebeck coefficient increases as we cross the structural phase transition and continues to increase with temperature until the presence of a downturn due to minority carrier contribution. The point at which the minority carrier contribution becomes significant shifts to a lower temperature during cooling. This feature remains regardless of the cycling and it presumably relates to the changes in composition as the sample traverses the phase diagram.

Finally, the resistivity values (Figure 3(c)) also decrease considerably after the first temperature cycle. During the third cycle, the resistivity values below the structural phase transition are $\rho \leq 1$ mΩ-cm, and above the transition the resistivity values on cooling remain <2 mΩ-cm. Above the structural phase transition, we also observe a continuous increase in the carrier concentration (Figure 3(b)) and a large drop in mobility (Figure 3(d)) that continues to decrease monotonically with increasing temperature. The mobility reduction explains the increase in the resistivity in the presence of increasing carrier concentration as the sample moves through the structural phase transition, and it is most likely due to the presence of mobile Ag ions. The carrier concentration at room temperature is $n = 4 \times 10^{18}\,\text{cm}^{-3}$ and at $T = 620$ K it reaches a value of $n = 1 \times 10^{19}\,\text{cm}^{-3}$. The mobility of $Ag_2Se_{0.5}Te_{0.5}$ is very high; the mobility values

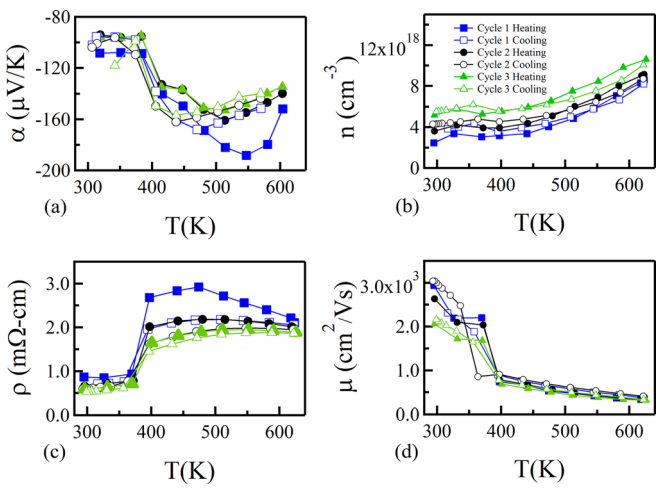

FIG. 3. (a) Seebeck coefficient, (b) carrier concentration, (c) resistivity, and (d) mobility of $Ag_2Se_{0.5}Te_{0.5}$ (sample 1). The solid markers correspond to the heating cycles, while the open markers correspond to the cooling cycles (squares–cycle 1, circles–cycle 2, triangles–cycle 3).

obtained are $\mu > 2000$ cm^2/Vs at room temperature and $\mu > 350$ cm^2/Vs at $T = 620$ K. Thus, the mobility of this highly disordered alloy is much greater than that of other state-of-the-art n-type thermoelectric materials. For comparison, the mobility of Te-doped Bi_2Te_3 is $\mu = 212$ cm^2/Vs,[25] and that of $La_{3-x}Te_4$ is $\mu = 4$ cm^2/Vs.[26] We only observe very small hysteresis in the mobility data above the phase transition, and the mobility values in that region do not vary with cycling. Hysteresis is only observed below the phase transition as the mobility in that region decreases with cycling. The carrier concentration on the other hand increases with cycling, in agreement with the reduction in resistivity, and the crossover temperature (temperature for which $n_{cooling} > n_{heating}$ on cooling) decreases. This crossover temperature appears to correlate with the temperature at which the bipolar contribution becomes significant.

The dimensionless figure-of-merit (zT) as a function of temperature is shown in Figure 4. The zT was calculated in the temperature region extending from 420 K to 610 K since this is the region of high thermoelectric efficiency (the zT values below the transition are of the order of $\sim$0.5 to 0.6). The large hysteresis observed between the heating and cooling curves is due to the hysteresis present in the Seebeck coefficient; the hysteresis in the electrical resistivity is reduced by cycling and the hysteresis in the thermal conductivity data remains small, but in the case of the Seebeck coefficient the hysteresis remains pronounced and persistent. As a result, significant hysteresis can be observed in the temperature region <520 K. The highest zT values are observed on cooling and in the temperature region <520 K. A consistent maximum $zT = 1.2$ is observed at $T = 440$ K. The maximum zT on cooling is observed in the case of sample 2 for which $zT = 1.4$ at 420 K, mainly due to a smaller value in the total thermal conductivity versus sample 1 at 420 K (on cooling, 0.47 W/mK versus 0.51 W/mK). Nonetheless, the large hysteresis observed in that temperature region suggests that the

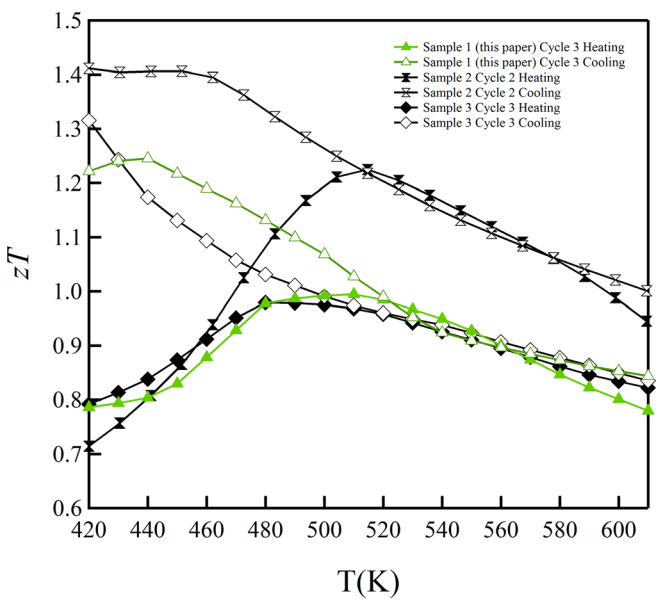

FIG. 4. zT as a function of temperature for 3 samples of $Ag_2Se_{0.5}Te_{0.5}$ (sample 1, sample 2, and sample 3). The solid markers correspond to the heating cycles, while the open markers correspond to the cooling cycles. The zT values were calculated using the data obtained in the last temperature cycle for each sample.

high zT values might be due to the formation of a metastable phase or kinetic effects resulting from the structural phase transition. However, zT in the non-hysteretic temperature region is very competitive ($zT = 1.0$ at $T = 520\,\mathrm{K}$ and $zT = 0.8$ at $T = 610\,\mathrm{K}$) and the lack of hysteresis between the heating and cooling curves suggests a stable alloy configuration. More importantly, the slow decrease in zT versus temperature ($d(zT)/dT \sim 0.0015\,\mathrm{K}^{-1}$) enables the potential for substantial waste heat recovery through a wide temperature region.

These results confirm that $Ag_2Se_{1-x}Te_x$ offers a very appealing compositional space that is conducive to high thermoelectric performance in the intermediate temperature regime. Specifically, the discussed composition (0.5/0.5) outperforms many of the state-of-the-art thermoelectric materials in the corresponding temperature range.[16] In addition, it provides an alternative system for the formation of biphasic alloys and the study of the effects of structural complexity and disorder on thermoelectric performance. Further studies are required in order to establish a correlation between the microstructure and the electrical and thermal transport behavior of these alloys to ultimately optimize their thermoelectric performance.

The authors would like to thank the U.S. Air Force Office of Scientific Research for supporting this work.

[1]F. J. DiSalvo, Science **285**, 703 (1999).
[2]A. D. LaLonde, Y. Z. Pei, H. Wang, and G. J. Snyder, Mater. Today **14**, 526 (2011).
[3]S. K. Mishra, S. Satpathy, and O. Jepsen, J. Phys. Condens. Matter **9**, 461 (1997).
[4]J. R. Salvador, J. Yang, X. Shi, H. Wang, and A. A. Wereszczak, J. Solid State Chem. **182**, 2088 (2009).
[5]X. Shi, J. R. Salvador, J. Yang, and H. Wang, Sci. Adv. Mater. **3**, 667 (2011).
[6]W. Wang, X. Yan, B. Poudel, Y. Ma, Q. Hao, J. Yang, G. Chen, and Z. Ren, J. Nanosci. Nanotechnol. **8**, 452 (2008).
[7]D. T. Morelli, V. Jovovic, and J. P. Heremans, Phys. Rev. Lett. **101**, 035901 (2008).
[8]H. J. Wu, S. W. Chen, T. Ikeda, and G. J. Snyder, Acta Mater. **60**, 6144 (2012).
[9]M. Ferhat and J. Nagao, J. Appl. Phys. **88**, 813 (2000).
[10]M. Fujikane, K. Kurosaki, H. Muta, and S. Yamanaka, J. Alloys Compd. **393**, 299 (2005).
[11]M. Fujikane, K. Kurosaki, H. Muta, and S. Yamanaka, J. Alloys Compd. **387**, 297 (2005).
[12]F. F. Aliev, M. B. Jafarov, and V. I. Eminova, Semiconductors **43**, 977 (2009).
[13]Y. Z. Pei, N. A. Heinz, and G. J. Snyder, J. Mater. Chem. **21**, 18256 (2011).
[14]J. Capps, F. Drymiotis, S. Lindsey, and T. M. Tritt, Philos. Mag. Lett. **90**, 677 (2010).
[15]T. B. Massalski and H. Okamoto, Binary alloy phase diagrams, ASM International, Materials Park, Ohio, 1990.
[16]G. J. Snyder and E. S. Toberer, Nature Mater. **7**, 105 (2008).
[17]H. J. Wu, S. W. Chen, T. Ikeda, and G. J. Snyder, Acta Mater. **60**, 1129 (2012).
[18]H. J. Wu, W. J. Foo, S. W. Chen, and G. J. Snyder, Appl. Phys. Lett. **101**, 023107 (2012).
[19]N. Aramov, I. Odin, and Z. Vonchevamladenova, Thermochim. Acta **20**, 107 (1977).
[20]S. Iwanaga, E. S. Toberer, A. LaLonde, and G. J. Snyder, Rev. Sci. Instrum. **82**, 063905 (2011).
[21]K. A. Borup, E. S. Toberer, L. D. Zoltan, G. Nakatsukasa, M. Errico, J. P. Fleurial, B. B. Iversen, and G. J. Snyder, Rev. Sci. Instrum. **83**, 123902 (2012).
[22]G. A. Wiegers, Am. Mineral. **56**, 1882 (1971).
[23]M. Kobayashi, Solid State Ionics **39**, 121 (1990).
[24]H. Wang, A. D. LaLonde, Y. Z. Pei, and G. J. Snyder, Adv. Funct. Mater. **23**, 1586 (2013).
[25]H. Scherrer and S. Scherrer, *Thermoelectrics Handbook* (CRC Press, Boca Raton, 1995).
[26]A. F. May, J.-P. Fleurial, and G. J. Snyder, Phys. Rev. B **78**, 125205 (2008).